Theoretical and Applied Fracture Mechanics 96 (2018) 418–427

Contents lists available at ScienceDirect

Theoretical and Applied Fracture Mechanics

journal homepage: www.elsevier.com/locate/tafmec

Residual stress measurements in offshore wind monopile weldments using neutron diffraction technique and contour method

Anais Jacob[a], Jeferson Oliveira[b], Ali Mehmanparast[a,*], Foroogh Hosseinzadeh[b], Joe Kelleher[c], Filippo Berto[d]

[a] Offshore Renewable Energy Engineering Centre, Cranfield University, Bedfordshire MK43 0AL, UK
[b] The Open University, Materials Engineering, Milton Keynes MK7 6BJ, UK
[c] Rutherford Appleton Laboratory, ISIS-STFC Facility, Chilton OX11 0QX, UK
[d] Norwegian University of Science and Technology (NTNU), Trondheim, Norway

ARTICLE INFO

Keywords:
Residual stress
Monopile
Fatigue crack growth
Offshore wind
Neutron diffraction
Contour method

ABSTRACT

Reliable assessment of the fatigue life of offshore wind monopiles operating in harsh offshore environments relies on quantifying the level of residual stresses locked-in at circumferential weld regions. This study presents, for the first time, residual stress characterisation, using the contour method, on a large structural welded mock-up, typical of the weldment used in offshore wind monopiles. The contour method and neutron diffraction measurements were also conducted on a compact tension specimen extracted from the large mock-up. The extracted compact tension sample, typically used for fracture and fatigue crack growth tests, showed notably significant remnant residual stresses that could impact fracture and fatigue test results. In addition the measured 2D map of transverse residual stresses, acting normal to the crack plane, playing a key role in fatigue crack opening/closure, exhibited variations through the thickness of the compact tension sample. The key conclusion was that the residual stresses in small laboratory samples extracted from large scale weldments should be carefully characterised and taken into account in structural integrity tests. Besides, the measurement results on the welded mock-up showed that the level of damaging tensile residual stress in large-scale mock-ups and hence real size structural welded monopiles is considerably larger than residual stresses in extracted laboratory samples; hence will have more significant influence on structural integrity of offshore wind assets.

1. Introduction

Renewable energy resources play a key role to mitigate greenhouse gas emissions, global temperature rises and provide energy security. Among renewable energy resources, wind energy is increasingly becoming one of the preferred sources of energy, particularly in Europe, with the potential for larger scale applications expanding rapidly. One of the important challenges in the offshore wind industry is the assessment of structural integrity of wind turbine foundations, which are becoming one of the largest engineering structures currently used in the energy sector.

Among the different types of existing offshore wind turbine support structures, monopile is the most popular foundation type which is widely used in shallow water offshore wind farms. Typical dimensions for the offshore wind turbine monopile range from 50 m to 70 m in length, 3 m to 10 m in diameter and 40 mm to 150 mm in wall thickness [1–3]. The primary function of a monopile is to support the offshore wind turbine structure. Monopiles are installed by driving them into the seabed; hence the structure should withstand the hammering loads during installation which vary from site to site depending on the soil conditions. During operation in harsh offshore environment, monopiles are subjected to wind, wave and sea current cyclic loads; hence they have to be designed for a certain fatigue life with suitable safety margins against failure. Moreover, they have to be designed to withstand the horizontal and vertical loads acting on the entire assembly including the transition piece, tower and wind turbine blades. Further details on the loading conditions and fatigue analysis of offshore wind monopiles can be found in the literature [4,5]. Monopiles are made of thick hot-rolled structural steel plates subjected to cold-rolling and bending followed by welding in the longitudinal direction to form “cans”. The individual cans are subsequently welded circumferentially to fabricate a full-length monopile.

It has been demonstrated by many researchers that welding residual stresses notably influence fatigue crack growth (FCG) behaviour of engineering materials. For example Lawrence et al. [6] have developed an analytical model to predict the influence of residual stress and stress

* Corresponding author.
E-mail address: a.mehmanparast@cranfield.ac.uk (A. Mehmanparast).

https://doi.org/10.1016/j.tafmec.2018.06.001
Received 25 January 2018; Received in revised form 24 April 2018; Accepted 11 June 2018
Available online 15 June 2018

Nomenclature

hkl	miller indices defining the lattice planes
λ	wavelength of the characteristic rays
d_{hkl}	lattice interplanar spacing of the crystal
$d_{0,hkl}$	lattice interplanar spacing of the strain-free sample
θ	incidence angle (Bragg's angle)
ε_{hkl}	residual strain corresponding to the *hkl* plane
ε_{err}	error in the strain measurements
d_{err}	error in the d-spacing measurements
σ_{err}	error in the residual stress measurements corresponding to ε_{err}
σ_{BM}	base metal yield stress
σ_{WM}	weld metal yield stress
E_{hkl}	Young's modulus of the *hkl* plane
ν_{hkl}	Poisson's ratio of the *hkl* plane
ΔK_{eff}	effective stress intensity factor range
ΔK_{th}	threshold stress intensity factor range
B	specimen thickness
M	mismatch ratio
N	number of cycles
W	specimen width
BM	base metal
WM	weld metal
C(T)	compact tension specimen geometry
HAZ	heat affected zone
PWHT	post-weld heat treatment
FCG	fatigue crack growth
RS	residual stress
TOF	time-of-flight
SCF	stress concentration factor

ratio on the fatigue life of a welded section. The main drawback of their model is that it is limited to crack initiation, and cannot account for welding residual stress effects on crack propagation behaviour of the material [6]. Moreover, the effects of compressive and tensile residual stresses on Mode I fatigue crack growth are discussed in [7] where residual stresses were introduced in the test specimens through shot peening. It has been demonstrated in references [7,8] that locked-in residual stresses alter the mean stress and also stress ratio under cyclic loading conditions and subsequently influence fatigue behaviour. Residual stresses particularly have more pronounced effects in near threshold region during FCG process and as the crack advances residual stresses redistribute and eventually vanish towards the end of the fatigue test [6–11]. It has been shown that the fatigue crack initiation and growth in monopile weldments occur primarily at circumferential welds due to the cyclic loads from wind and wave that offshore wind turbines are subjected to [12]. A significant effort has been made in the SLIC JIP (Structural Lifecycle Industry Collaboration Joint Industry Project) to characterise the FCG behaviour of these welded structures in air as well as in seawater in order to better estimate the remaining life of monopiles based on laboratory scale FCG tests on base metal (BM) and weldments (i.e. weld metal (WM) and heat affected zone (HAZ)) [9,10]. The SLIC project has successfully developed FCG curves to investigate the fatigue behaviour of offshore wind welded steel foundations. However, due to the lack of data available at the time, the effect of residual stress on FCG particularly in the near threshold region was not considered in the analysis and therefore was proposed as an important future work.

There is a significant research gap in reliable characterisation of the state of residual stress in monopile structures upon fabrication, after pile drilling, during service operation and indeed the effect of welding sequence on residual stresses in monopiles [11–17]. In addition, the weld quality itself plays a significant role in the fatigue life of welded components [18]. There is currently high level of uncertainty and conservatism in the existing codes and standards for the design process or lifetime and structural integrity assessment of monopiles due to the lack of consideration of residual stress effects. This is particularly crucial due to the fact that unlike many other industries such as nuclear no post weld heat treatment is performed on monopiles because of the size and cost issues. Moreover, it is quite well known that residual stress measurement results from laboratory scale specimens are not easily transferable to components, due to the size effects and therefore different constraint levels, which subsequently result in different residual stress states. Hence, it is recommended to test samples at quite high stress ratios (i.e. $R = 0.5$) to imply comparably high tensile residual stresses and supply a conservative transfer of laboratory scale test specimen results to welded components and structures.

In order to remove the uncertainty and conservatism in the structural design and integrity assessment of monopiles, welding residual stresses need to be reliably characterised at the fabrication, installation and operation stages leading to reliable estimate of fatigue crack initiation and propagation in monopiles particularly at circumferential weld regions in which the cracks are often first created.

In this paper, for the first time, we present residual stress characterisation using the contour method on a large welded mock-up, in the form of a plate, typical of offshore wind monopile weldment. We also conducted neutron diffraction and contour method measurements on a compact tension, C(T), specimen extracted from the large welded mock-up. C(T) fracture mechanics test specimens are typically used in characterising FCG behaviour of engineering materials in lab environments. The following sections explain the details of the test specimens and the residual stress measurement techniques performed in this work. The results from these measurements are presented and discussed in terms of the effect of residual stress on fatigue crack growth behaviour of monopile weldments in small-scale laboratory samples and real-size scale structures.

2. Specimens

2.1. A large welded mock-up

The material used for the large mock-up is EN-10225:09 S355 G10 + M, which is widely used in the fabrication of offshore structures including offshore wind turbine monopiles [19]. The chemical composition of the base metal used in this work, which has the Carbon

Table 1
Chemical composition of the base metal.

Element, wt%										
C	Si	Mn	P	S	N	Cu	Mo	Ni	Cr	
0.061	0.280	1.58	0.013	0.0007	0.0041	0.254	0.006	0.342	0.034	
V	Nb	As	Sn	Ti	Pb	B	Sb	Ca	Bi	Al-T
0.001	0.022	0.003	0.001	0.003	0.00	0.0003	0.001	0.0028	0.0001	0.032

Equivalent of 0.372%, is given in Table 1. To replicate the existing welds in monopiles for the mock-up, multi-pass submerged arc welding (SAW) tandem-twin process was chosen to increase deposition rates and productivity. The solid wire electrode was EN ISO 14171-A (EN 756): S3Si and the chosen flux was EN ISO 14174: SA FB 1 55 AC H. Multi-pass welding was conducted on double V-grooved hot-rolled plates with 90 mm thickness, 800 mm length (in longitudinal direction) and 1300 mm width (in transverse direction). The plates were welded by EEW in Germany who are one of the leading manufacturers of monopile foundations in Europe. Welding was conducted parallel to the rolling direction using run off, thereafter cut, at each end of the plate as shown in Fig. 1. No post-weld heat treatment (PWHT) was performed in order to replicate real-life conditions of offshore wind monopile structures. A macrograph of the weld is shown in Fig. 2, where the three regions of interest (BM, WM, HAZ) have been revealed and labelled.

The welding process began with the edge preparation where two large parent plates were placed next to each other and the first V-groove was machined. Then the tack welds were performed on the inside section followed by the outer section with a pre-heat of 60 ^{0}C. The weld run sequence started on the inside of the first milled groove and was gradually directed towards the external surface, using up to 3 electrode wires providing a heat input of up to 3.0 kJ/mm and an inter-pass temperature of not more than 250 ^{0}C. Gas burners were used for pre-heating the plates and the temperature was measured by thermo crayons. 18 weld beads were applied in total in the first V-groove. Once the first V-groove was welded, the plate was rotated 180° and the second V-groove was machined. Welding on the second V-groove began with the same sequence running from the inside of the notch to the outside, with 25 weld beads being applied in total. The schematic welding sequence for the first and second V-groove is shown in Fig. 3. It must be noted that in the fabrication of monopiles the weld toes of the plates are either in flush ground or as-welded conditions [16]. The current study is focused on as-welded plates without grinding of the weld-toes thus taking into consideration the worst case scenario (greatest stress concentration factors).

To facilitate transport of the welded plate, the width (transverse dimension), after welding was reduced from 2600 mm to 600 mm by flame cutting at approximately 300 mm from and at either side of the weld region. The length of the plate along the longitudinal direction was reduced by flame cutting to 600 mm. The section for contour method residual stress characterisation was measured 90 mm (thickness) × 600 mm (in longitudinal direction) × 600 mm (in transverse direction). A smaller section with 90 mm (thickness) × 200 mm (in longitudinal direction) × 600 mm (in transverse direction) dimensions was prepared for the extraction of a C(T) specimen and also tensile specimens. It is worth noting that the welded plate sections were transported with great care to minimise the vibration, environmental, and temperature variation effects, during transportation on the residual stress state. Moreover, as discussed in Section 3.3, the flame cut regions were selected to be sufficiently away from the weld region to minimise the effect of flame cutting on the residual stress profiles near the weld toes.

2.2. Tensile and C(T) specimens

In order to characterise the tensile behaviour of the material used in this study, a cross-weld tensile specimen, comprising of the BM, WM and HAZ, with the cross sectional area of 8 × 8 mm^2 was extracted from the 90 mm × 200 mm × 600 mm welded section as shown in Fig. 4. The tensile test was performed at room temperature with the displacement rate of 1 mm/min. The tensile force was continuously recorded during the test and the strain distributions were monitored using the digital image correlation (DIC) technique. A Dantec Q400 DIC system was used to record the displacement within each of the three regions at the surface of the tensile specimen [20]. The tensile curve obtained from this test is shown in Fig. 5, where the engineering stress is plotted against the engineering plastic strain. Due to the resolution of the DIC technique, only plastic strains in the BM, HAZ and WM were measured from the DIC test. The measured 0.2% proof stress is 455 MPa for the BM, 469 MPa for the HAZ and 477 MPa for the WM. To measure elastic properties of the material, an additional tensile test on a round bar sample extracted from the BM was conducted and the Elastic Young's modulus and Poisson's ratio were found to be $E = 196$ GPa and $\nu = 0.3$, respectively. In this work it was assumed that the elastic properties of the WM and HAZ are the same as the BM. The tensile test results in Fig. 5 show that the current weld studied in this research is slightly overmatched and the mismatch ratio ($M = \sigma_{WM}/\sigma_{BM}$) is just above unity.

Compact tension C(T) specimens are typically used to characterise fracture properties and fatigue crack propagation behaviour of materials. C(T) specimens extracted from larger weldments are often assumed to be stress-free, hence the effect of any remnant residual stress on characterised fatigue or fracture behaviour is often mistakenly ignored. In order to investigate the level of remaining residual stresses in fracture mechanics specimens extracted from the large welded mock-up, a 20 mm thick slice was extracted from the 90 mm × 200 mm × 600 mm welded section, ground, polished and subsequently etched using 10% Nital solution in order to visualise the weld and HAZ zones. Previous studies [12] have shown that the crack initiation in monopiles mainly occurs at the weld toe (in the as-welded condition) and in the HAZ region of the circumferential weld and propagates into the BM in through-thickness direction, due to lateral wind and wave loads, as schematically shown in Fig. 6. As discussed in [12] the fatigue crack initiation and propagation in the HAZ needs to be characterised. Therefore, a standard C(T) specimen with the width of $W = 50$ mm, thickness of $B = 16$ mm and height of $H = 60$ mm [21] was extracted from the ground, polished and etched slice of the extracted 90 mm × 200 mm × 600 mm welded section with the initial crack tip located in the middle of the HAZ region similar to the procedure detailed in [12]. It must be noted that a thicker sample with $B = 20$ mm was initially extracted from the welded section from which a 4 mm thick slice was machined off for d_0 measurements. The extracted C(T) specimen and its orientation with respect to the welded plate is shown in Fig. 7. As illustrated in this figure, the loading condition for the extracted C(T) is parallel to the transverse welding direction to replicate the loading conditions in monopiles. This is consistent with the C(T) specimen orientations tested in [12]. The FCG rates for offshore wind turbine monopiles in air and in seawater for a structural steel grade, welded with similar procedure as this work, have been previously characterised in the SLIC project [12] though the remaining welding residual stresses in C(T) specimens were not measured

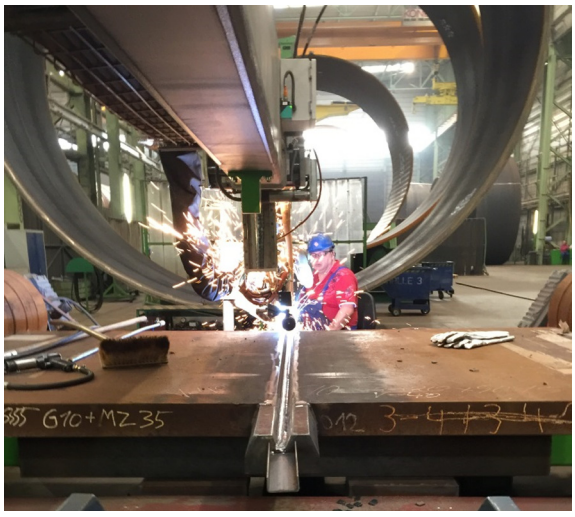

Fig. 1. Multi-pass submerged arc welding on S355 G10 + M welded mock-up.

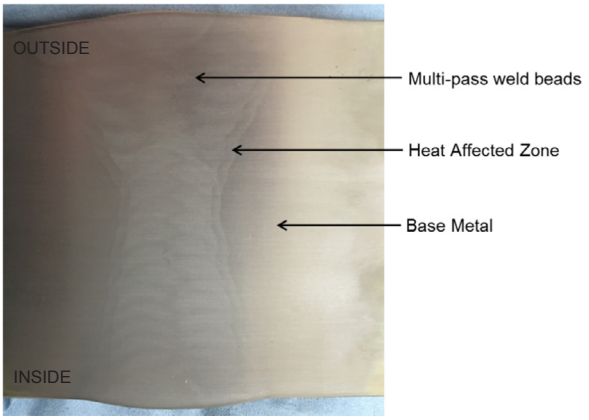

Fig. 2. Weld macrograph following polishing and etching the surface of cross-weld extracted slice.

and considered in the analysis; Hence the influence of residual stresses on fatigue crack growth behaviour of monopile weldments particularly in the near threshold region could not be investigated. The current study mainly focuses on characterising the transverse residual stress in the extracted C(T) specimen, which is parallel to the loading direction of the C(T) sample and perpendicular to the crack plane.

3. Residual stress measurements

In the present work, the extracted C(T) sample was first measured non-destructively in three principal directions using neutron diffraction technique. The contour method measurement was then performed to provide 2-Dimensional (2D) map of transverse residual stresses over the plane of crack growth for future fatigue tests. Note that the measurements were performed on a C(T) specimen with the machined V-notch tip and prior to pre-fatigue cracking. The contour method was also conducted on the large welded mock-up along a transverse plane to measure longitudinal residual stresses in the as-welded condition.

3.1. Neutron diffraction measurement on the C(T) sample

Neutron diffraction measurements were performed on Engin-X instrument at the Rutherford Appleton Laboratory spallation source in Didcot, UK. At Time-Of-Flight (TOF) instruments, pulsed neutrons are produced in time intervals and neutron speed is measured by timing their passage over a known distance. Moreover, the angle of scattering is fixed, since a single pulse contains a continuous spectrum of wavelength, and the time-of-flight is proportional to the lattice spacing [22]. In crystalline materials, diffractometers measure the atomic interplanar spacing, where a specific volume is lit and the diffracted neutrons are recorded [23]. A schematic of the neutron diffraction measurement set up is presented in Fig. 8. In these measurements, the diffraction angle, θ, is kept fixed and the lattice deformation at different peaks is measured following the Bragg's law [24]:

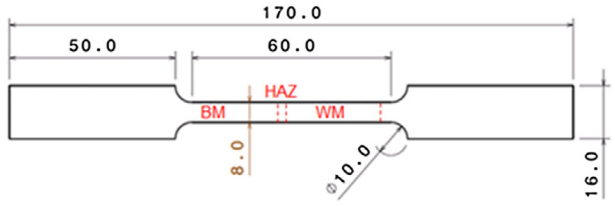

Fig. 4. Tensile test specimen dimensions (all dimensions are in millimetres).

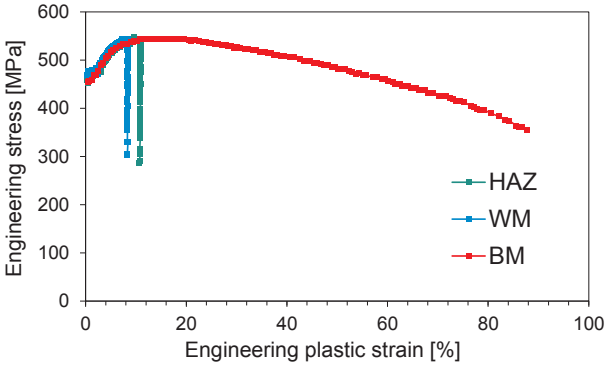

Fig. 5. Cross-weld DIC tensile test results for the BM, HAZ and WM.

$$n\lambda = 2d_{hkl}\sin\theta \tag{1}$$

where *hkl* are the Miller indices defining the lattice planes, n is a constant, λ is the wavelength of the characteristic rays, d_{hkl} is the lattice interplanar spacing of the crystal and θ is the incidence angle (Bragg's angle).

Thereafter, the residual strains can be calculated using the following equation:

$$\varepsilon_{hkl} = \frac{d_{hkl} - d_{0,hkl}}{d_{0,hkl}} \tag{2}$$

where ε_{hkl} is the residual strain corresponding to the *hkl* plane, d_{hkl} is the lattice interplanar spacing of the crystal measured and $d_{0,hkl}$ is the lattice interplanar spacing of the strain-free sample.

The error in the strain measurements are also calculated as follow:

$$\varepsilon_{err} = \sqrt{\frac{d_{err}^2}{d^2} + \frac{d_{0,err}^2}{d_0^2}} \tag{3}$$

where ε_{err} is the error in the strain measurements, d_{err} is the error in the d-spacing measurements and $d_{0,err}$ is the error in the d-spacing measurements of the strain free sample.

Consequently, the residual stresses can be calculated using the equation below [25].

$$\sigma_i = \frac{E_{hkl}}{1+\nu_{hkl}}\varepsilon_i + \frac{\nu_{hkl}E_{hkl}}{(1+\nu_{hkl})(1-2\nu_{hkl})}(\varepsilon_1+\varepsilon_2+\varepsilon_3) \tag{4}$$

where σ_i is the residual stress corresponding to ε_i residual strain, E_{hkl} is

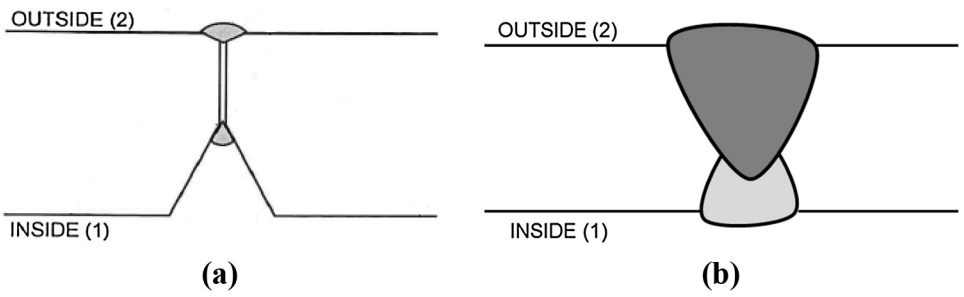

Fig. 3. (a) Edge preparation of the welding sequence with inside/outside tack welds milled out (b) weld run sequence.

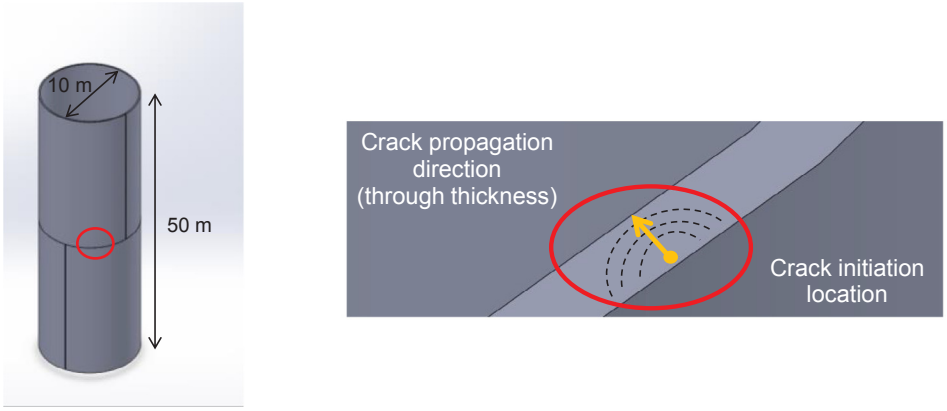

Fig. 6. (a) A schematic representation of a circumferential weld in an offshore wind turbine monopile (b) Representation of the crack initiation and propagation within a circumferential weld of a monopile.

the Young's modulus of the *hkl* plane, ν_{hkl} is the Poisson's ratio of the *hkl* plane, ε_1 is the residual strain in the first direction (e.g. longitudinal), ε_2 is the residual strain in the second direction (e.g. transverse) and ε_3 is the residual strain in the third direction (e.g. normal).

The error in the residual stress is calculated as per the following equation:

$$\sigma_{erri} = \sqrt{\left(\frac{E_{hkl}}{1+\nu_{hkl}}\varepsilon_{erri}\right)^2 + \left(\frac{\nu_{hkl}E_{hkl}}{(1+\nu_{hkl})(1-2\nu_{hkl})}\right)^2 \times (\varepsilon_{err1}^2 + \varepsilon_{err2}^2 + \varepsilon_{err3}^2)} \quad (5)$$

where σ_{erri} is the error in the residual stress measurements, corresponding to the error in the residual strain measurements ε_{err}, ε_{err1} is the error in the strain measurement in the first direction (e.g. longitudinal), ε_{err2} is the error in the strain measurement in the second direction (e.g. transverse) and ε_{err3} is the error in the strain measurement in the third direction (e.g. normal).

Residual stress measurements were performed using a gauge volume of $2 \times 2 \times 2\,mm^3$ at the mid-thickness and mid-height of the sample, along the crack propagation direction (i.e. specimen symmetry line) and the lattice spacing, *d*, was measured along longitudinal, transverse and normal directions. Note that in neutron diffraction measurements on Engin-X, the lattice spacing at each point can be measured along two directions. Therefore, in the first set of measurements, the lattice spacing was measured along normal and longitudinal directions in the North bank and the South bank, respectively. After the sample rotation by 90°, the second set of measurements were conducted to measure lattice spacing along transverse and longitudinal directions using the North and South banks, respectively.

As seen in Eq. (2), an error in d_o measurement will significantly affect the accuracy of residual strain and subsequently residual stress values obtained from neutron diffraction measurements. In order to minimise the error in d_o measurements in this work, 10 small cubes of $3 \times 3 \times 3\,mm^3$ were extracted from the exact same region of the crack path in the main C(T) specimen using Electro Discharge Machining (EDM) technique. A thicker sample than a standard C(T) blank was initially extracted from the welded section. A 4 mm thick slice was machined off from the C(T) blank from which the individual stress-free cubes were extracted. These extracted cubes for strain-free measurements and their exact location with respect to the crack growth

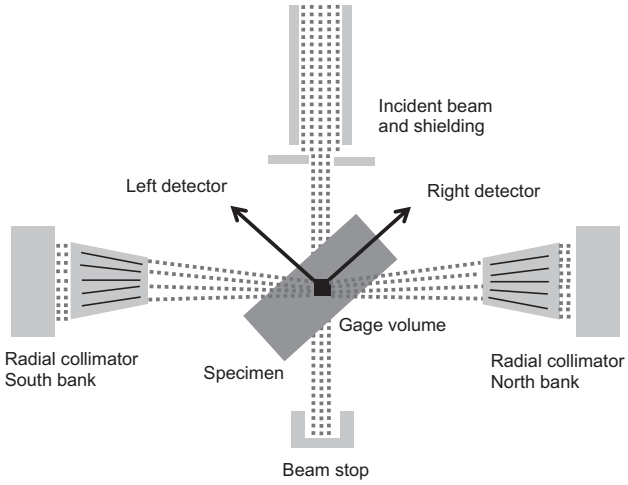

Fig. 8. Schematic demonstration of neutron diffraction measurement set up.

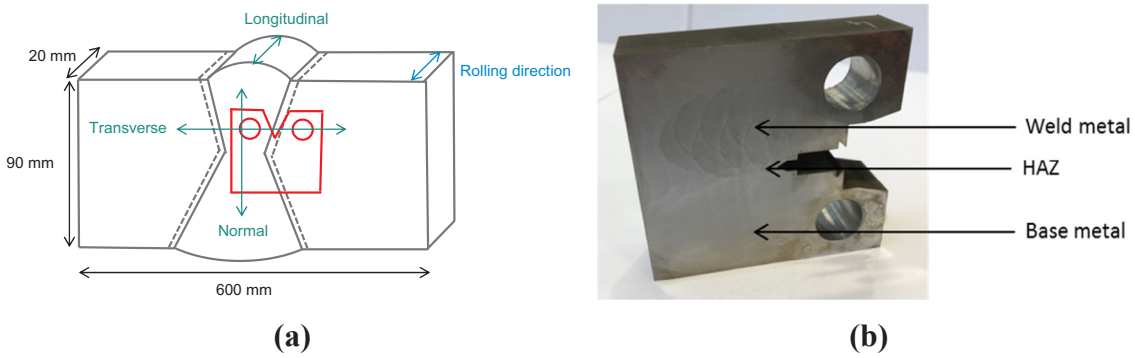

Fig. 7. (a) C(T) specimen extraction location with respect to the welded mock-up (b) Compact tension, C(T), specimen extracted from the welded slice.

direction in C(T) specimen are shown in Fig. 9. The numbering of the cubes is to record the order of the extracted cubes with respect to the distance from the crack tip in the main C(T) sample. d_0 measurements were performed on individual cubes and their orientation specific values were recorded in North and South banks. The residual strains were calculated using Eq. (2) and subsequently residual stresses were calculated in all three directions. Note that for residual stress measurements, the analysis was performed by applying the Pawley fit [26], which is often used to analyse the neutron diffraction data for welded samples e.g. [27–29], to the obtained d-spacing data for different lattice planes and employing elastic bulk properties of $E = 196$ GPa and $\nu = 0.3$ in the analysis [30].

The residual strain and residual stress measurements in all three directions from the C(T) specimen are presented against distance from the crack (notch) tip in Fig. 10 and Fig. 11, respectively. It is evident from Fig. 11 that there is high level of compressive residual stresses at the notch tip with the largest magnitude observed in the normal direction. Transverse residual stress of around -200 MPa is measured at the notch tip, which is expected to influence the fatigue crack growth behaviour of the material, particularly at the early stages of the test. Ahead of the crack tip, along the expected crack propagation line at mid-thickness, there can be observed variation in the measured residual stress profiles. However, the trend of the transverse and normal residual stress profiles in particular, is overall in compression.

3.2. Contour residual stress measurement on the C(T) sample

The contour method (CM) of residual stress measurement involves carefully cutting the specimen of interest using wire EDM (electro-discharge machining), measuring the out of plane deformation profile of the newly created cut faces, averaging the measured deformation profiles from the two cut parts, filtering out experimental noise, applying the reverse of the averaged smoothed profile as nodal displacement boundary conditions in an FE (finite element) model of the cut part and finally performing an elastic stress analysis [31]. The back calculated stresses on the cut surface obtained from the FE modelling step is a true representation of the residual stress component acting normal to the cut plane that was present in the sample prior to performing the cut.

The contour method measurement on the C(T) sample was performed over the plane of expected fatigue crack growth; that is a longitudinal cut plane to measure transverse stresses (see Figs. 7 and 12). An Agie Charmilles Cut 1000 EDM machine with a 50 µm diameter brass wire was used to perform the contour cut. Prior to the cut, a layer of sacrificial material was attached to the top and bottom surfaces using electrically conductive glue to mitigate the wire entry and exit cutting artefacts [32] (see Fig. 13). The sample was securely clamped to the

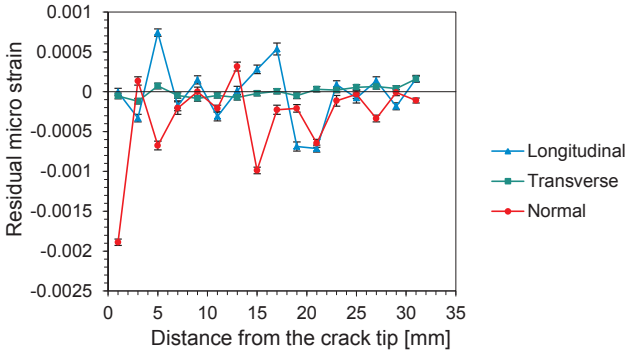

Fig. 10. Residual strain measurements on the C(T) sample using neutron diffraction technique.

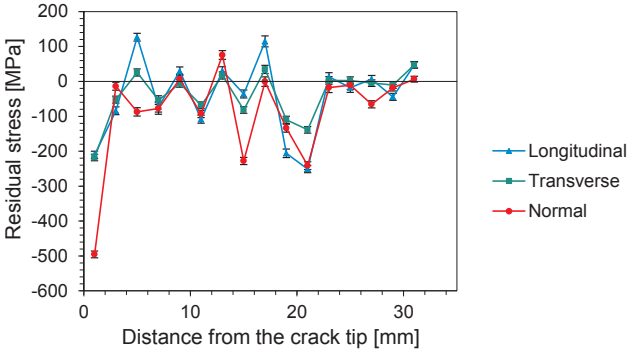

Fig. 11. Residual stress measurements on the C(T) sample using neutron diffraction.

EDM stage (see Fig. 13), which was then filled with deionised water and left to reach thermal equilibrium before starting the cut.

The cut surfaces were cleaned using acetone, isopropanol, and a soft brush and placed in the metrology lab to reach thermal equilibrium with the ambient air. A Zeiss Eclipse co-ordinate measuring machine (CMM), fitted with a Micro-Epsilon laser probe and a 2 mm diameter ruby-tipped Renishaw PH10M touch trigger probe was used for surface deformation measurements. The surface profile of both cut surfaces was measured using the laser probe with an in-plane point spacing of 25 µm adopted. In addition, the perimeters of the two cut parts were measured with the touch-probe and later used for precisely aligning the measurements of the two cut parts before averaging the profiles and for creating an accurate FE model geometry.

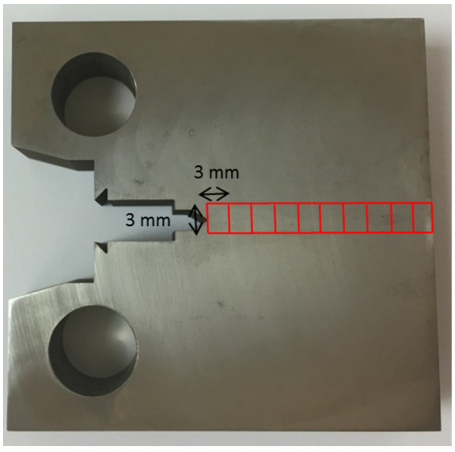

(a)

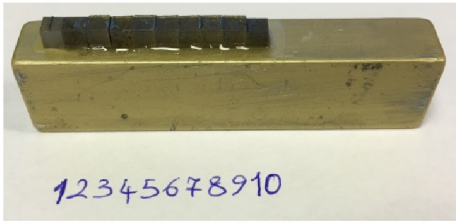

(b)

Fig. 9. (a) Extraction pattern of the strain free samples for d_0 measurements (b) Strain free cube samples numbered from 1 to 10.

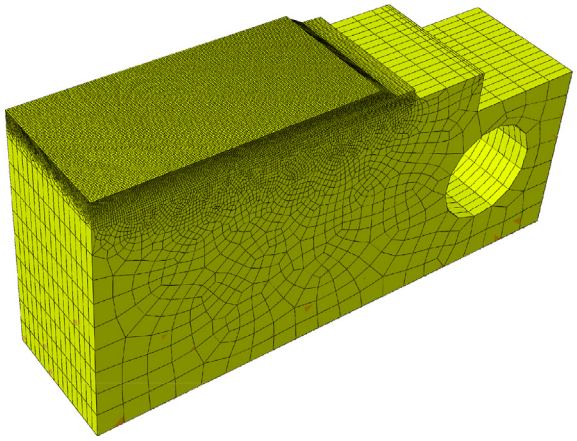

Fig. 12. Illustration of the mesh of the FE model used in the contour method residual stress determination of the C(T) sample.

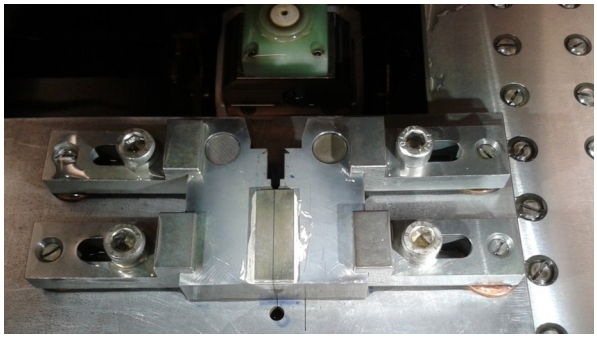

Fig. 13. Clamping arrangement for the EDM cutting step of the contour method on the C(T) sample. The photo also shows the sacrificial layer on the top surface.

To calculate the displacement profile, the data sets for opposing cut surfaces were aligned using the measured perimeters and then interpolated onto a common grid before averaging to remove errors due to shear stress and possible anti-symmetric cutting artefacts [31]. Due to the uncertainty in CMM measurements and the roughness of the EDM cut surfaces, noise in the displacement profile is unavoidable and it would be further amplified in the stress calculation. Therefore, the profile was smoothed using a median filter (StressMap's proprietary algorithm). The smoothing level was modulated by varying the 'mask size' between 0.275 and 2.025 mm in steps of 0.25 mm and the optimum smoothing level within this range was given by a mask size of 1.525 mm. For this mask size, the overall fitting error, estimated using the approach in [33], was just over 7 MPa.

To calculate the stresses, an FE model was created in Abaqus 6.13 with the geometry of one of the cut halves (see Fig. 12). The model was meshed using linear hexahedral elements with reduced integration (C3D8R). The mesh at the cut surface was biased from 0.25 mm near the surface of interest up to 3 mm on the opposite face. The model was assigned uniform isotropic elastic properties, with a Young's modulus of 196 GPa and Poisson's ratio of 0.3. The smoothed displacement profile,

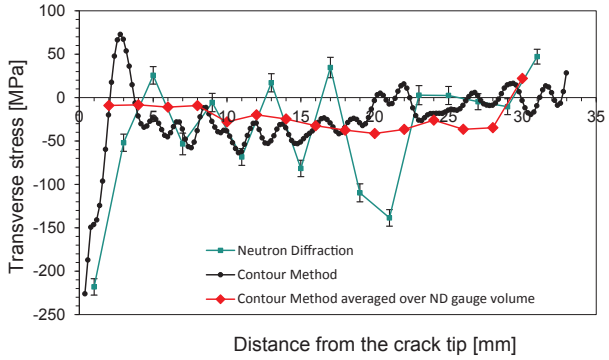

Fig. 15. Comparison of transverse residual stress measurements on the C(T) specimen using neutron diffraction and the contour method.

with a reverse sign, was applied as surface boundary condition on the surface nodes of the FE model of the cut parts and an elastic stress analysis was performed. The 2D map of transverse residual stress obtained from the contour method, see Fig. 14, provides a rich set of information about the distribution of residual stress over the expected plane of crack growth in the C(T) sample. The contour map showed the presence of high compressive residual stress at the central region through the thickness of the sample near the crack tip with much lower level of residual stresses further ahead of the notch. An important observation from the 2D cross-sectional map of transverse residual stress is the variation of transverse residual stress through the thickness of the sample.

The transverse stresses measured using the contour method and neutron diffraction for a line profile at mid-thickness of the C(T) sample are compared in Fig. 15. Similar to neutron diffraction measurements, the contour method showed the presence of high level of compressive transverse residual stress of around -200 MPa at the crack tip. It is worth noting that neutron diffraction gives averaged stresses over the measured gauge volume (in this case 2 mm × 2 mm × 2 mm). Therefore, in order to compare the results on a fair basis, an additional line profile for the contour method is provided in Fig. 15 where the contour stresses are averaged over the neutron diffraction gauge area. Both the local contour stress line profile and the contour stress line profile averaged over neutron diffraction gauge volume confirmed that transverse residual stresses ahead of the crack tip are predominantly in compression and the level of stresses is less than -50 MPa further ahead of the crack tip.

3.3. Residual stress measurements on the welded mock-up

For the large welded mock-up the contour method was conducted on a transverse plane at mid-length to map 2D distribution of longitudinal stresses. An Agie Charmilles FI 440 ccS EDM machine was used to perform the cut using a 250 μm diameter brass wire. The sample was firmly clamped to the EDM stage, which was then filled with deionised water and left to reach thermal equilibrium before starting the cut. To mitigate plasticity and the so-called bulge error [34–36], the main cut through the weld was performed between two pilot holes and the remaining ligaments were cut afterwards (as shown in Fig. 16).

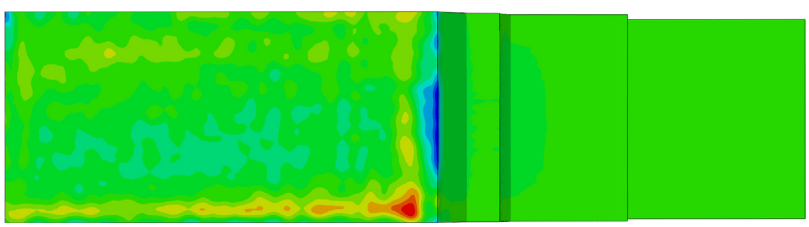

Fig. 14. Contour residual stress measurement results along transverse direction of the weld on the C(T) specimen. The stress scale is in MPa.

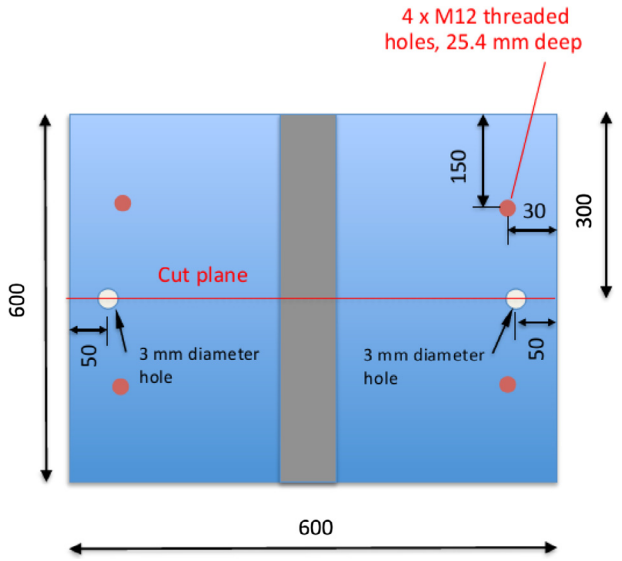

Fig. 16. Dimensions of the welded mock-up showing the location of the contour cut plane and pilot holes. The drawing is not scaled and all dimensions are in millimetres.

The cut surfaces were cleaned and then measured with the same CMM equipment described earlier, with an in-plane point spacing of 100 µm. In addition, the perimeters of the two cut parts were measured with the touch-probe. The standard data analysis approach as explained earlier was performed on the measured surface deformations. Fig. 17 shows the averaged displacement profile prior to smoothing. The smoothing level was modulated by varying the 'mask size' of a median filter (StressMap's proprietary algorithm) between 3.1 and 10.1 mm in steps of 1 mm and the optimum smoothing level within this range was given by a 6.1 mm mask size. For this mask size, the overall fitting error, estimated using the approach in [33], was less than 5 MPa.

The FE model to back calculate the stresses, see Fig. 18, was meshed using linear hexahedral elements with reduced integration (C3D8R). The mesh on the cut surface was biased from 1 mm near the weld up to 3.5 mm away from the weld. A bias was also applied in the extrusion direction, going away from the cut face, from 0.5 up to 50 mm. The model was assigned uniform isotropic elastic properties, with a Young's modulus of 196 GPa and Poisson's ratio of 0.3. The smoothed displacement profile, with a reverse sign, was applied as boundary condition on the surface nodes of the simulated cut parts. The resulting 2D map of the stress component normal to the cut surface represents the initial residual stresses distribution acting longitudinally to the weld (see Fig. 19). It can be seen that there are two distinct regions of tensile stress within the weld, which correlate to the double-groove welding sequence. Compressive stresses are observed on the top and bottom faces of the plate away from the weld, while high tensile stresses are present towards the ends of the cross-section (extreme left and right-hand-sides). The compressive stresses, observed at top and bottom

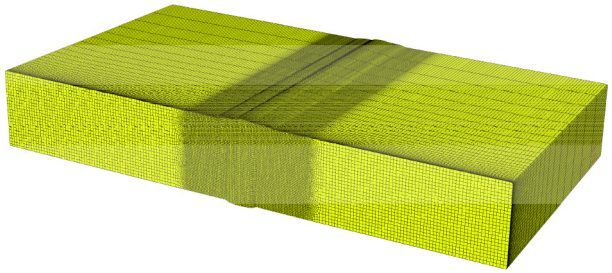

Fig. 18. Illustration of the mesh of the FE model used in the contour method residual stress determination of the welded mock-up.

faces, are believed to have been introduced as a result of the rolling process that the plates were subjected to before welding. In addition, these compressive stresses may have been intensified to balance the tensile stresses introduced due to the welding process elsewhere within the cross-section. The tensile residual stresses towards the ends of the plate are believed to be the result of the flame cutting operation that was performed to extract the 600 mm × 600 mm sample out of the larger (2600 mm × 800 mm) welded mock-up. Note that these near surface tensile residual stresses at two ends of the plate are sufficiently away from the weld region with insignificant penetration depth, confirming that the flame cuts had negligible effects on the residual stress profiles near the weld toes. Due to the presence of pilot holes, no deformation data was recorded adjacent to the pilot holes, see Fig. 17. As a result the provided stress map in these regions is masked and the resulting stress data should not be reported, see Fig. 19.

4. Discussion

4.1. Residual stress effects on fatigue behaviour of C(T) specimen

The study carried out on a C(T) specimen extracted from a welded plate has shown a non-uniform distribution of transverse residual stresses on the crack plane (i.e. compressive at the mid-thickness and tensile at the outer surfaces). This varying through-thickness residual stress distribution profile subsequently influences the crack propagation rate profile leading to uncertainties in crack growth monitoring in fracture mechanics specimens. The crack length measured on the outer surface may differ to the crack length at the mid-thickness, depending on the residual stress distribution profile. As the crack propagates, residual stresses redistribute and are likely to slowly vanish. However, the presence of residual stress significantly influence the effective threshold stress intensity factor range, $\Delta K_{eff,th}$, and hence influence the crack initiation and early crack propagation. Therefore, more pronounced effects from residual stresses are expected on the fatigue crack initiation and early stage fatigue crack propagation. The re-distribution of residual stresses during the FCG tests on C(T) specimens extracted from monopile weldments is beyond the scope of this paper and will be examined in future work.

Moreover, the locked-in welding residual stresses and their

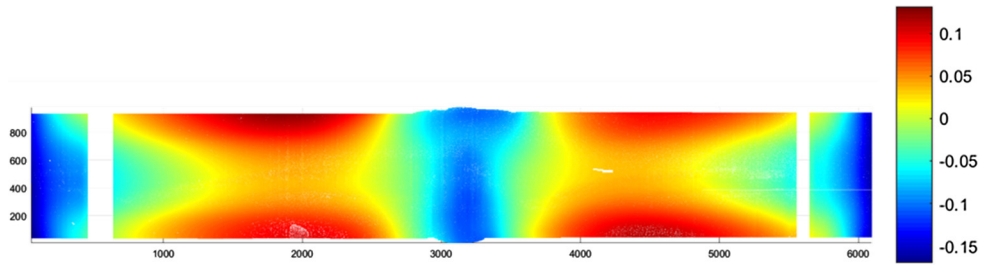

Fig. 17. Map of the averaged surface deformation of the cut surfaces for the contour method. Deformation unit is in millimetres. Plate dimensions are in 10 × millimetres.

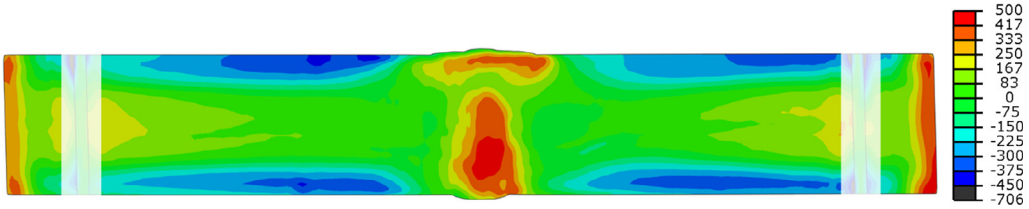

Fig. 19. Longitudinal residual stress measurement obtained from the contour method. The stress unit is in MPa.

redistribution during FCG tests will change the *R*-ratio (stress ratio), the mean stress and effective stress intensity factor range, ΔK_{eff}. The effectiveness of mean stress conditions on the fatigue response of welded components is investigated in [37] where the presented results give an insight into the optimization of the welding parameters in order to improve the fatigue life of welded components. The results obtained from this study have shown that in order to accurately characterise fatigue crack initiation and propagation behaviour in monopile welded structures, realistic values of residual stresses which are much greater than the remaining residual stresses in C(T) specimens must be considered in structural testing and analyses.

4.2. Residual stress effects on fatigue behaviour of monopile

A comparison of the residual stresses in longitudinal direction between the C(T) specimen, measured using neutron diffraction technique, and the large welded mock-up, measured using the contour method, is given in Fig. 20. In order to accurately compare both measurements the results from the welded plate have been taken within the region exactly where the C(T) sample was extracted from. As seen in Fig. 20, the longitudinal residual stresses measured on the C(T) sample are significantly lower than those in the welded plate as they tend to vanish and redistribute during the specimen extraction process. The residual stress reduction due to sample extraction has also been noted and discussed by other researchers in [38,39]. The results from the literature and the current study demonstrate that although specimen extraction reduces the residual stress levels, the hypothesis for future work is that a substantial amount of residual stresses still remain in the extracted samples which can play a significant role in laboratory scale FCG tests on C(T) fracture mechanics specimens. Therefore, these stresses need to be measured and considered in the FCG data analysis. Thermo-mechanical weld simulations and numerical analysis of specimen extraction from welded plates, to predict the remaining residual stress profile in fracture mechanics C(T) specimens, is the subject of a future work following on the present study.

A comparison of the measurements results obtained within the welded plate and the C(T) sample in Fig. 20 shows that the longitudinal residual stress in the welded plate (300 MPa on average) is significantly greater than the longitudinal residual stress in the C(T) sample (in the order of -50 MPa). Although the normal and transverse components of the residual stresses on the welded mock-up are not available and will be measured in future work, a similar scaling factor might be expected in residual stress measurements in transverse direction between the welded mock-up and the C(T) sample. This implies that the transverse residual stresses at circumferential welds in monopiles can be very large and close to the yield stress of the material which subsequently result in accelerated crack initiation and propagation under corrosion-fatigue loading conditions. According to [40] and based on the measurements performed, it appeared that the maximum and minimum residual stress levels that can occur after welding may be up to the yield strength of the material. The worst case scenario would present tensile residual stress with a magnitude of about the yield stress of the material which would inevitably lead to crack initiation and propagation and therefore fatal fracture.

5. Conclusions

The design and structural integrity codes and standards for offshore wind structures do not take into account explicitly the effect of residual stresses. This current study presents residual stress characterisation in structural steel offshore wind monopile weldments using neutron diffraction technique and the contour method. For the first time the contour method of residual stress measurement was conducted on a large welded mock-up with typical welding procedure used in the fabrication of monopile structural weldments. This was followed by conducting neutron diffraction and contour method measurements on a standard C(T) specimen extracted from the welded mock-up. The residual stress measurements revealed a significant redistribution and reduction in the level of residual stresses by extracting laboratory samples from large scale welded structures. The remnant residual stresses in the standard laboratory samples are significant enough to have potential impacts on fatigue crack initiation, in particular, and crack propagation of future fatigue tests. The contour method measurement on the large welded mock-up showed significantly large level of tensile residual stress in the welded structure in the as-welded condition. This close to yield magnitude of tensile residual stress, if not reliably treated or accounted for in structural integrity assessments, could inevitably lead to accelerated fatigue crack initiation and propagation and unexpected catastrophic failure of monopile structures.

Acknowledgements

This work was supported by grant EP/L016303/1 for Cranfield University and the University of Oxford, Centre for Doctoral Training in Renewable Energy Marine Structures - REMS (http://www.rems-cdt.ac.uk/) from the UK Engineering and Physical Sciences Research Council (EPSRC). Furthermore, valuable contributions of all members of staff involved in neutron diffraction measurements at Rutherford Appleton Laboratory and contour measurements at the Open University are greatly appreciated. In particular, discussions with Prof. John Bouchard from the Open University and Prof. Feargal Brennan from Cranfield University are greatly acknowledged.

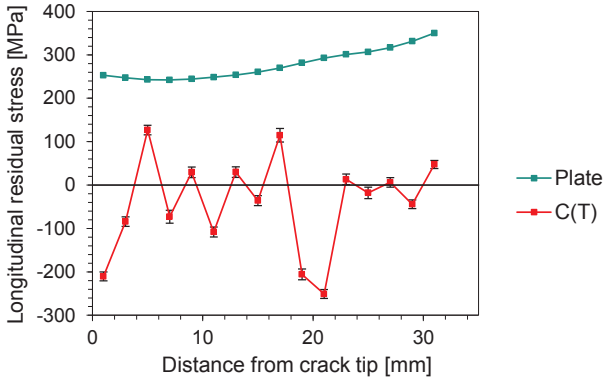

Fig. 20. Comparison of longitudinal residual stresses in the C(T) specimen measured using neutron diffraction technique and in the welded plate measured using the contour method.

Appendix A. Supplementary material

Supplementary data associated with this article can be found, in the online version, at http://dx.doi.org/10.1016/j.tafmec.2018.06.001.

References

[1] J. Velarde, Design of monopile foundations to support the DTU 10 MW offshore wind turbine, 2016.
[2] J. Van Der Tempel, Design of support structures for offshore wind turbines (PhD thesis), 2006.
[3] L. Arany, S. Bhattacharya, J. Macdonald, S.J. Hogan, Design of monopiles for offshore wind turbines in 10 steps, Soil Dyn. Earthq. Eng. 92 (2016) 126–152.
[4] J. Peeringa, G. Bedon, Fully integrated load analysis included in the structural reliability assessment of a monopile supported offshore wind turbine, Energy Procedia 137 (2017) 255–260.
[5] J. Velarde, E.E. Bachynski, Design and fatigue analysis of monopile foundations to support the DTU 10 MW offshore wind turbine, Energy Procedia 137 (2017) 3–13.
[6] F.V. Lawrence, J.D. Burk, J.-Y. Yung, Influence of residual stress on the predicted fatigue life of weldments, Residual stress effects in fatigue, 1982, pp. 33–43.
[7] D.V. Nelson, Effect of residual stress on fatigue crack propagation, Residual stress effects in fatigue, (1982).
[8] J. Baumgartner, Enhancement of the fatigue strength assessment of welded components by consideration of mean and residual stresses in the crack initiation and propagation phases, Weld. World 60 (3) (2016) 547–558.
[9] X. Lu, Influence of Residual Stress on Fatigue Failure of Welded Joints, NC State University, 2003.
[10] P.-Y. Cheng, Influence of Residual Stress and Heat Affected Zone on Fatigue Failure of Welded Piping Joints, NC STate University, 2009.
[11] J. Krebs, M. Kassner, Influence of welding residual stresses on fatigue design of welded joints and components, Weld. World 51 (7/8) (2007) 54–68.
[12] A. Mehmanparast, F. Brennan, I. Tavares, Fatigue crack growth rates for offshore wind monopile weldments in air and seawater: SLIC inter-laboratory test results, Mater. Des. 114 (2017) 494–504.
[13] O. Adedipe, F. Brennan, A. Mehmanparast, A. Kolios, I. Tavares, Corrosion fatigue crack growth mechanisms in offshore monopile steel weldments, Fatigue Fract. Eng. Mater. Struct. 40 (11) (2017) 1868–1881.
[14] B. Maier, C. Guster, R. Tichy, W. Ecker, Different microstructures in the HAZ of double submerged arc welded pipelines and how they influence the fatigue crack growth, Proceeding of the ASME 2013 Pressure Vessels & Piping Division Conference, (2013).
[15] A. Mehmanparast, O. Adedipe, F. Brennan, A. Chahardehi, Welding sequence effects on residual stress distribution in offshore wind monopile structures, Frat. ed Integrità Strutt. 35 (2016) 125–131.
[16] Det Norske Veritas AS, Fatigue Design of Offshore Steel Structures, 2005.
[17] The British Standards Institution, BSI Standards Publication Guide to methods for assessing the acceptability of flaws in metallic structures, 2015.
[18] B. Jonsson, G. Dobmann, A.F. Hobbacher, M. Kassner, G. Marquis, IIW Guidelines on Weld Quality in Relationship to Fatigue Strength, Springer International Publishing, Cham, 2016.
[19] Det Norske Veritas AS, Offshore Standard DNV-OS-B101: Metallic Materials, 2009.
[20] B. Pan, K. Qian, H. Xie, A. Asundi, Two-dimensional digital image correlation for in-plane displacement and strain measurement: a review, Meas. Sci. Technol. 20 (2009) 62001–62017.
[21] ASTM International, Standard test method for measurement of fatigue crack growth rates, 2010.
[22] IAEA International Atomic Energy Agency, Measurement of residual stress in materials using neutrons, Proceedings of a technical meeting, (2003).
[23] R. Woracek, Energy selective neutron imaging for the characterization of polycrystalline materials, University of Tennessee, 2015.
[24] R. Pynn, Neutron scattering - a non-destructive microscope for seeing inside matter, Neutron scattering applications and techniques, Springer, 2009.
[25] A. Mehmanparast, C.M. Davies, K.M. Nikbin, Quantification and prediction of residual stresses in creep crack growth specimens, Mater. Sci. Forum 777 (2014) 25–30.
[26] G.S. Pawley, Unit-cell refinement from powder diffraction scans, J. Appl. Crystallogr. 14 (6) (1981) 357–361.
[27] S. Pratihar, M. Turski, L. Edwards, P.J. Bouchard, Neutron diffraction residual stress measurements in a 316L stainless steel bead-on-plate weld specimen, Int. J. Press. Vessel. Pip. (86) 13–19.
[28] M.E. Kartal, C.D.M. Liljedahl, S. Gungor, L. Edwards, M.E. Fitzpatrick, Determination of the profile of the complete residual stress tensor in a VPPA weld using the multi-axial contour method, Acta Mater. 56 (16) (2008) 4417–4428.
[29] J.R. Santisteban, M.R. Daymond, J.A. James, L. Edwards, ENGIN-X: A third-generation neutron strain scanner, J. Appl. Crystallogr. 39 (6) (2006) 812–825.
[30] M.T. Hutchings, P.J. Withers, T.M. Holden, T. Lorentzen, Introduction to characterization of residual stress by neutron diffraction, (8) (2005).
[31] M.B. Prime, Cross-sectional mapping of residual stresses by measuring the surface contour after a cut, J. Eng. Mater. Technol. 123 (2) (2001) 162.
[32] F. Hosseinzadeh, P. Ledgard, P.J. Bouchard, Controlling the cut in contour residual stress measurements of electron beam welded Ti-6Al-4V alloy plates, Exp. Mech. 53 (5) (2013) 829–839.
[33] M.B. Prime, R.J. Sebring, J.M. Edwards, D.J. Hughes, P.J. Webster, Laser surface-contouring and spline data-smoothing for residual stress measurement, Exp. Mech. 44 (2) (2004) 176–184.
[34] F. Hosseinzadeh, Y. Traore, P.J. Bouchard, O. Muránsky, Mitigating cutting-induced plasticity in the contour method, part 1: Experimental, Int. J. Solids Struct. 94–95 (2016) 247–253.
[35] O. Muránsky, C.J. Hamelin, F. Hosseinzadeh, M.B. Prime, Mitigating cutting-induced plasticity in the contour method. Part 2: Numerical analysis, Int. J. Solids Struct. 94–95 (2016) 254–262.
[36] M.B. Prime, A.L. Kastengren, The contour method cutting assumption: error minimization and correction, Exp. Appl. Mech. 6 (2010).
[37] M. Leitner, Influence of effective stress ratio on the fatigue strength of welded and HFMI-treated high-strength steel joints, Int. J. Fatigue 102 (2017) 158–170.
[38] C.D.M. Liljedahl, O. Zanellato, M.E. Fitzpatrick, J. Lin, L. Edwards, The effect of weld residual stresses and their re-distribution with crack growth during fatigue under constant amplitude loading, Int. J. Fatigue 32 (4) (2010) 735–743.
[39] K.A. Venkata, C.E. Truman, D.J. Smith, R.C. Wimpory, Relaxation of residual stresses when extracting a specimen from a dissimilar metal electron beam welded plate, 7th international conference on creep, fatigue and creep-fatigue interaction, 2016, pp. 19–22.
[40] Y.-H. Zhang, S. Smith, W. Liwu, C. Johnston, Residual stress measurements and modelling, Fatigue Fract. Eng. Mater. Struct. 40 (2017) 1868–1881.